Compressive strength of an unsaturated granular material during cementation

Jean-Yves Delenne, Fabien Soulié, Moulay Saïd El Youssoufi, Farhang Radjai

Compressive strength of an unsaturated granular material during cementation

J.-Y. Delenne, F. Soulié, M.S. El Youssoufi, F. Radjai

LMGC UMR 5508 CNRS-Université Montpellier 2,
cc048 Place Eugène Bataillon, 34095 Montpellier cedex, France

Abstract

The cohesive behaviour of unsaturated granular materials is due to the presence of cohesive bonds between grains. These bonds can have various physico-chemical characteristics and may evolve with environmental conditions. We study the case of a granular material partially saturated by an aqueous solution. The bonds are thus initially of capillary type and the mechanical strength is weak. At low relative humidity, the phase change of water involves crystallization of the solute at the contact points between grains, generating thus solid bonds. The mechanical strength of the material is then enhanced. An experimental study of the evolution of the mechanical strength during crystallization of the solute shows clearly the transition from capillary regime to cemented regime. This transition is not correlated with the mass of the crystallized solute, but rather with the residual degree of saturation. This behavior is analyzed here in the light of discrete element simulations. We introduce a local cohesion law that accounts for transition from capillary to cemented bonding. This law is formulated in terms of the degree of crystallization as a result of the evaporation of water at the boundary of the sample. The cohesion of the packing is initially of capillary type. A crystallization front then spreads from the sample boundaries to the center of the sample, and the strength increases as a result. Uniaxial compression allows us to determine the strength at different times. The numerical strength agrees well with the experimental data, and reveals strength enhancement as the solute crystallizes, as well as the transition from capillary to cementation regime.

Keywords: Unsaturated granular materials, capillary cohesion, cemented bonds, Discrete Element Method

1. Introduction

The mechanical strength of granular materials is controlled by particle characteristics (shape, size distribution) and cohesive bonding (capillary, cementation) between the particles. The effect of these parameters is of primary importance in powder technology [1, 2, 3] and transformations of geomaterials including granular soils [4, 5, 6]. The liquid is generally water with various impurities and/or dissolved minerals that can crystallize and reinforce the mechanical strength of the material. The mechanical strength can thus evolve as a result of phase changes (evaporation and crystallization) depending on the surrounding hygrothermic conditions.

In this paper, we investigate the evolution of the compressive strength of unsaturated granular materials during the evaporation of a solvent. A cohesion law is proposed in which the debonding force is a function of a crystallization index accounting for liquid-solid transition at the scale of a cohesive bond. This law is implemented in 2D discrete element method (DEM) simulations of simple compression in the course of drying. The results are compared with the experimental data obtained on model materials tested in similar conditions.

2. Experiments

The experimental tests were designed to measure the compressive strength of granular samples during the process of the drying and deposition of a solute at the liquid bridges between the grains. Two types of materials were used in these tests: (1) a model material composed of glass beads and (2) Ventoux sand (Fig. 1). In both cases, the grains were first washed and dried. Then, they were sieved to keep only the grains with diameters in the range from 0.4 mm to 0.8 mm. The dry grains were homogeneously mixed with a small amount of saturated brine containing 35.6 g of NaCl for 100 g of water at room temperature. This maximum concentration varies with temperature [11, 12].

The samples (diameter 25 mm and height 17 mm) were prepared inside a cylindrical mould of a diameter of 25 mm and a height of 17 mm. At this stage the samples are particularly delicate to handle since their mechanical strength is solely ensured by weak capillary forces acting between the grains.
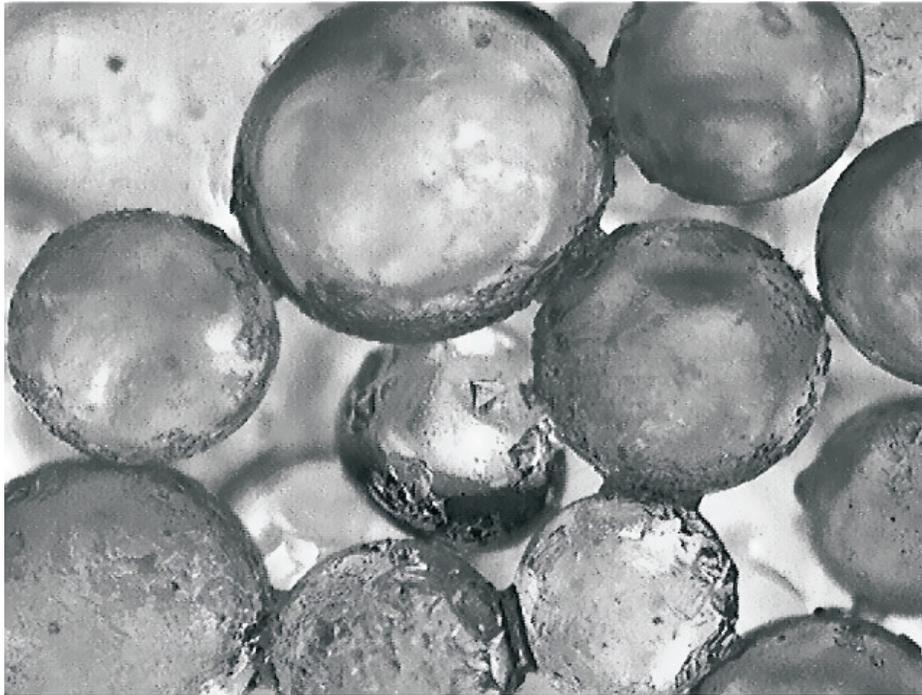
Figure 1: Distribution of liquid bridges and NaCl deposits in a granular material composed of glass beads.
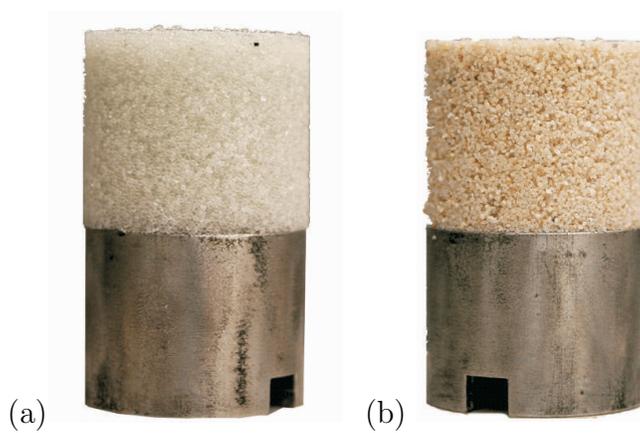
Figure 2: Samples during drying (a) glass beads and (b) sand of Ventoux.

Because of this brittleness, particular experimental precautions were necessary in order to avoid damage to the samples upon unmoulding. In the course of drying, the samples are first weighed ; the mass difference gives access to the mass of the evaporated water and thus that of the crystallized fraction of salt. The samples are then subjected to unconfined vertical compression up to failure in order to determine their mechanical strength. Figure 3 clearly illustrates the evolution of the mechanical strength with drying and thus the progressive cimentation of the solute.

3. Local crystallization law

We consider a liquid bridge of an aqueous solution connecting two grains. This solution contains a solute with a given initial concentration. Depending on the surrounding drying conditions, the water progressively evaporates and the solute concentration increases. When the saturation point is reached, the solute begins to crystallize as the water further evaporates. The first solid deposits are localized on the grain surface. The solid-bond connectivity between the grains is obtained when a sufficient amount of solute is crystallized and a cemented bond is formed. As drying continues, the cemented bond gets thicker and stronger.

The order parameter for phase transition at the scale of a bond is the ratio i defined by

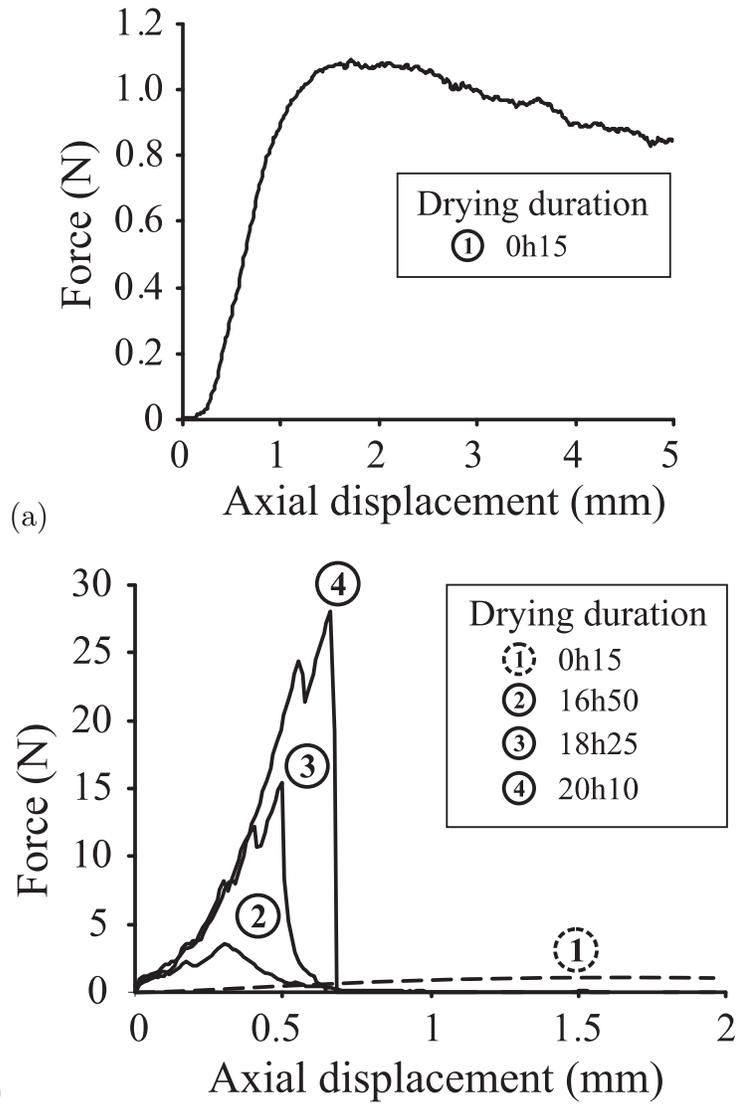$$i = \frac{m}{m_{tot}} \tag{1}$$

Figure 3: Results of axial compression tests for several drying durations: (a) Low drying, bonds are mainly liquid bridges ; (b) Illustration of the effect of the progressive cementation on the mechanical strength.

5

where m is the mass of crystallized solute and m_{tot} is the total mass of solute available in the bond. In the following, we will refer to i as *crystallization index*. The index i is a field variable depending on the time t elapsed since the beginning of drying and the location $\vec{r}$ of each bond. Below the saturation point, i is identically zero. At saturation, i begins to increase with evaporation first at the free surface, and tends to 1 at long times while at the same time the crystallization front spreads into the sample from the free surface. The evolution of $i(t, \vec{r})$ can be modeled as a diffusive process:

$$i = \gamma \left\{ 1 - \frac{4\pi r}{(2+\pi)L} e^{-\left(\frac{\pi}{2L}\right)^2 Dt} \right\} \qquad (2)$$

where $r = \|\vec{r}\|$ is the smallest distance between the bond and the free surface, L is a characteristic dimension of the macroscopic sample, and D is a diffusion coefficient. This coefficient represents the crystallized solute propagation rate in the sample. Since the liquid is saturated by the solute, D is directly related to the diffusion of water vapor in the sample. The coefficient γ describes whether the solution is saturated ($\gamma = 1$) or not ($\gamma = 0$).

The debonding force f_n^Y is a function only of the crystallization index i. As long as i is below a critical value i_T, the bond behavior is governed by the liquid phase and thus the debonding force is given by the capillary force f_l. At $i = i_T$, a solid bridge forms and the behavior of the bond turns to solid. In our numerical model, we assume that the debonding force in this regime, i.e. for $i \geq i_T$, is a linear function of i with a maximum f_s reached in the limit $i \to 1$. With this approximation, the debonding force is given by

$$f_n^Y = f_l + H(i - i_T) \frac{i - i_T}{1 - i_T}(f_s - f_l) \qquad (3)$$

where H is the Heaviside step function. This law captures in a simple way the effect of crystallization. The two thresholds f_s and f_l depend on the local geometry (gap, size polydispersity), volume fraction of the solution and solid-liquid contact angle. But, we are interested here in the evolution of the bond, and it will be assumed that the values of f_s and f_l are constant.

4. Numerical procedures

We used 2D DEM simulations with usual elastic-frictional contact interactions together with a cohesion law described by Eq. 3 [8, 9, 10]. We assume

Parameter	Value	Unit
Contact stiffness K_n	10^{-6}	N/m
Time step Δt	$5\ 10^{-7}$	s
Compression velocity v	$1\ 10^{-3}$	m/s
Friction coefficient μ	0.2	
Capillary force f_l	$1.3\ 10^{-4}$	N
Maximum solid force f_s	$4.5\ 10^{-3}$	N
Diffusion coefficient D	$2.5\ 10^{-9}$	m^2/s

Table 1: Parameters and values used for DEM simulations.

that the aqueous solution is saturated, so that $\gamma = 1$ and the characteristic dimension L equals the sample's radius (Eq. 2). The values of various simulation parameters are given in table 1. The samples are composed of 5100 spherical grains with diameters following a gaussian distribution in the range 0.4 mm to 0.8 mm. These numerical samples have a rectangular shape (17 mm high and 25 mm wide). They are subjected to unconfined vertical compression test at a low velocity $v = 10^{-3}$ m/s.

The simulations were actually designed to reproduce 3D experiments that were carried out with packings of glass beads and sand as described in section 2. The crystallized fraction of salt is the global index of crystallization I, which is the average value of crystallization index i ($I = \frac{1}{V} \int_V i\, dV$), where V is the volume of the sample. Both in experiments and simulations, the failure force F is measured for different values of I. The experimental value of the transition index is estimated to be $i_T = 0.8 \pm 0.1$. Hence, three different systems with $i_T = 0.7$, 0.8 and 0.9 are simulated.

5. Macroscopic behavior

Figure 4 displays the snapshots of the two sets of simulated configurations. In both cases, we observe the propagation of the crystallization front from the free boundary toward the center of the sample. The central zone is subject only to capillary cohesion. The stress field is macroscopically inhomogeneous due to the presence of the capillary zone surrounded by the cemented zone. The normal forces are stronger along two vertical stripes in the cemented zone. When the front reaches the center of the sample, all bonds are cemented, but crystallization continues within the bonds.

The evolution of the failure force F, normalized by the failure force F_l due to capillary bonds at the beginning of the simulation, as a function of the global crystallization index I is shown in Fig. 5. We see that for a given value of I, the failure force is higher for smaller values of i_T. Two regimes can be distinguished: 1) $I < i_T$: The normalized force F grows slowly from 1 to $\simeq 8$ as I varies from 0 to i_T. This regime corresponds roughly to the propagation of the crystallization front from the free surface to the center of the sample. 2) $I > i_T$: F grows fast and tends to $F \simeq 40$. This regime corresponds to the consolidation of cemented bonds throughout the system.

Figure 6 shows the evolution of the failure force F with I for both experiments and simulations. All the experimental data points collapse nearly on the same curve for glass beads and sand irrespective of the initial brine content. The simulation data are presented as a range (hashed zone) defined by $0.7 \geq i_T \geq 0.9$. The experimental data belong mostly to this range, showing that the simulations capture correctly the transition from liquid to solid behavior despite the 2D geometry of the simulations.

The high value of compressive strength ($F \simeq 40$) when $I \rightarrow 1$ has two different origins. On one hand, at the scale of a bond, we have $f_s \simeq 35 f_l$. On the other hand, in contrast to a liquid bond which involves only a tensile strength in addition to sliding friction, a solid bond involves rolling (or bending) strength as well as tensile strength. The rolling strength is crucial for compressive strength of cohesive granular materials [13].

6. Conclusion

In this paper, we proposed a numerical model for the evolution of cohesion in an unsaturated granular material due to the crystallization of a solute. We introduced an order parameter i defined as the fraction of crystallized solute. Hence, the evolution of a bond between two particles is described by a cohesion law expressing the the tensile force as a function of this order parameter. This law involves both a transition from capillary to cemented bond and the consolidation of a cemented bond as the order parameter increases.

Our discrete element simulations with this evolutive cohesion law show that the compressive strength grows with drying from a free surface and a transition occurs from a regime dominated by capillary cohesion to a regime governed by cemented bonds. The numerical simulations are in good agreement with experiments on glass beads and sand with a brine of variable content in salt. Experiments are presently under way in order to characterize in
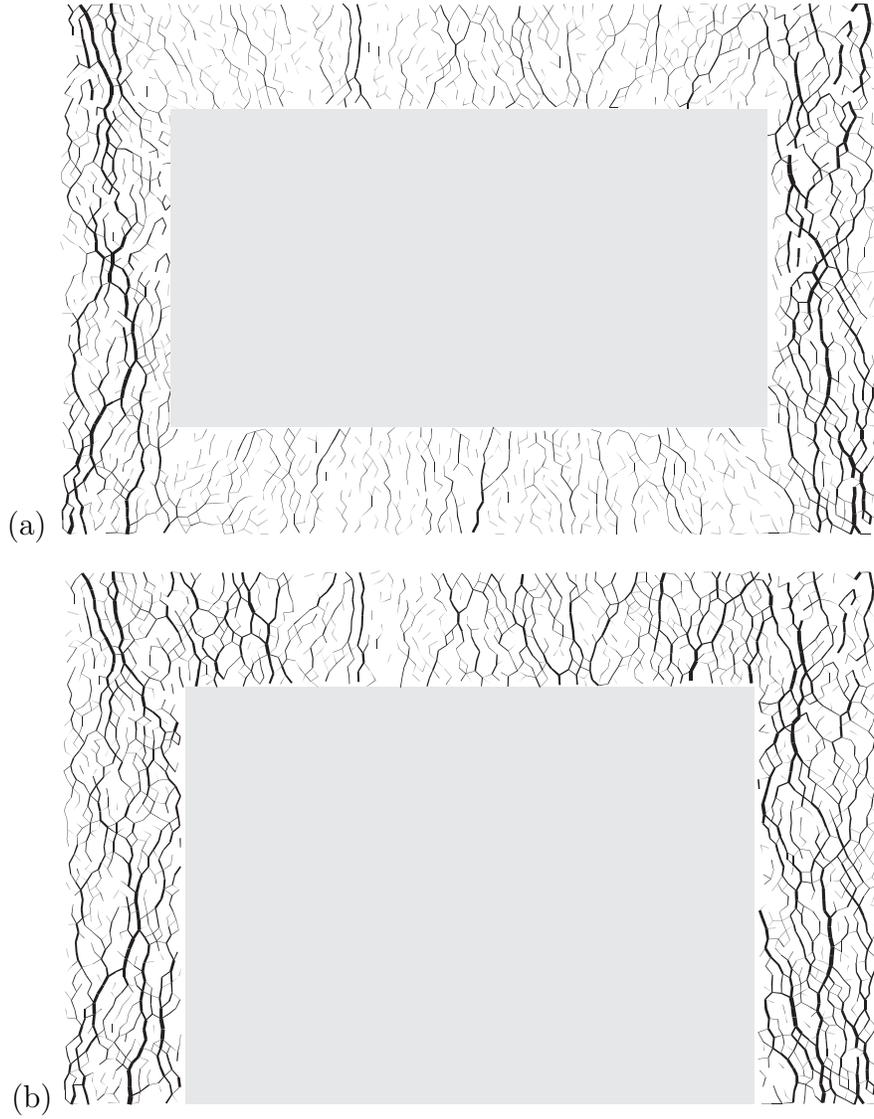
8

Figure 4: Compressive forces in the cemented zone for the two sets of configurations simulated: (a) simulations of S1 configuration; (b) simulations of S2 configuration. Line thickness is proportional to normal force.
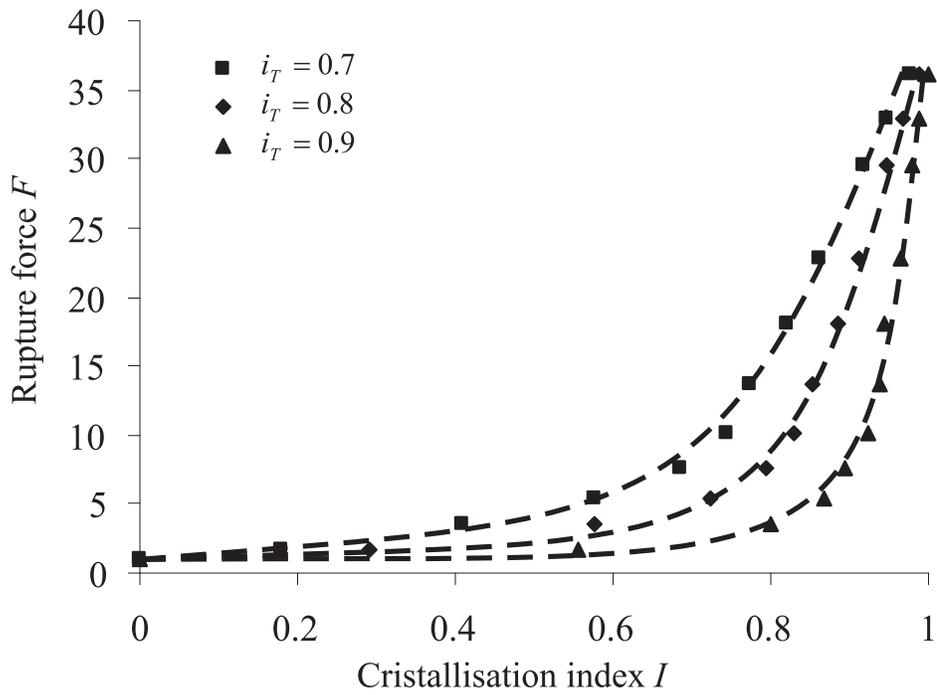
Figure 5: Evolution of the failure force F, normalized by the failure force F_l due only to capillary forces at the beginning of simulation, with the global crystallization index I for three different values of the local transition index i_T.
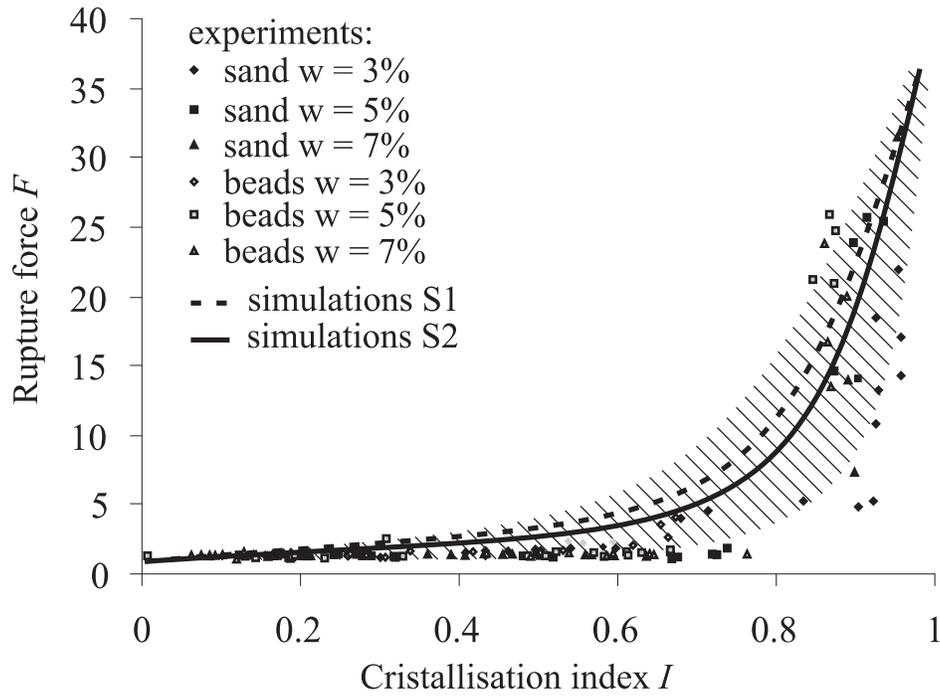
Figure 6: Evolution of failure force F normalized by F_l with the global crystallization index I. Comparison between DEM simulations and experiments for different materials and liquid contents w (the figure shows a synthesis of 82 tests carried out on glass beads and 60 tests carried out on sand). The hashed zone represents the simulations for i_T in the range $[0.7, 0.9]$.

more detail the local evolution law of cohesion as a function of surrounding hygrothermic and physico-chemical conditions.

[1] S. Iveson, J. Litster, B. Ennis, Fundamental studies of granule consolidation. part 1: Effects of binder content and binder viscosity, Powder Technology 88 (1996) 15–20.

[2] S. Iveson, J. Litster, K. Hapgood, B. Ennis, Nucleation, growth and breakage phenomena in agitated wet granulation processes: A review, Powder Technology 117 (2001) 3–39.

[3] A. Nokhodchi, An overview of the effect of moisture on compaction and compression, Pharmaceutical Technology 29 (1) (2005) 46–66.

[4] C. Cardell, F. Delalieux, K. Roumpopoulos, A. Moropoulou, F. Auger, R. V. Grieken, Salt-induced decay in calcareous stone monuments and buildings in a marine environment in SW france, Construction and Building Materials 17 (2003) 165–179.

[5] B. Lubelli, R. V. Hees, C. Groot, The role of sea salts in the occurrence of different damage mechanisms and decay patterns on brick masonry, Construction and Building Materials 18 (2004) 119–124.

[6] L. Rijniers, L. Pel, H. Huinink, K. Kopinga, Salt crystallization as damage mechanism in porous building materials-a nuclear magnetic resonance study, Magnetic Resonance Imaging 23 (2005) 273–276.

[7] F. Soulie, M. S. El Youssoufi, J.-Y. Delenne, C. Voivret, C. Saix, Effect of the crystallization of a solute on the cohesion in granular materials, Powder Technology 175 (2007) 43–47.

[8] J.-Y. Delenne, M. S. El Youssoufi, F. Cherblanc, J.-C. Bénet, Mechanical behaviour and failure of cohesive granular materials, International Journal for Numerical and Analytical Methods in Geomechanics 28 (2004) 1577–1594.

[9] F. Soulie, F. Cherblanc, M. S. El Youssoufi, C. Saix, Influence of liquid bridges on the mechanical behaviour of polydisperse granular materials, International Journal for Numerical and Analytical Methods in Geomechanics 30 (2006) 213–228.

[10] V. Richefeu, M.S. El Youssoufi, F. Radjai, Shear strength properties of wet granular materials, Physical Review E 73 (051304) (2006) 1–11.

[11] D. Kaufmann (Ed.), Sodium chloride, the production and properties of salt and brine, Reinhold Publishing Corporation, New York, 1960.

[12] H. Langer, H. Offermann, On the solubility of sodium chloride in water, Crystal Growth 60 (1982) 389–392.

[13] N. Estrada, A. Taboada, F. Radjai, Shear strength and force transmission in granular media with rolling resistance, Physical Review E 78, (021301) (2008) 1–11.